Urol Res (2011) 39:165–170
DOI 10.1007/s00240-010-0316-z

ORIGINAL PAPER

Preliminary feasibility study of FTIR microscopic mapping system for the rapid detection of the composited components of prostatic calculi

Ted Hueih-Shing Hsu · Shan-Yang Lin · Chih-Cheng Lin · Wen-Ting Cheng

Received: 24 April 2010 / Accepted: 24 July 2010 / Published online: 22 October 2010

Abstract Awareness of the chemical composition of prostatic calculi is of great importance for pathogenesis of prostatic lithiasis, the feasibility of FTIR microspectroscopic mapping system used for rapidly screening and detecting the real composited components of prostatic calculi in a short time was initially evaluated. Prostatic calculi were retrieved during transurethral resection of the prostate from nine patients diagnosed having benign prostatic hyperplasia with lower urinary tract symptoms. The level of serum prostatic-specific antigen was within 0–12.63 ng/ml. The calculi samples were examined and compared using FTIR microspectroscopic mapping system, or the traditional FTIR and Raman microspectroscopies. The traditional FTIR microspectroscopic results indicate that nine calculi samples mainly consisted of carbonated HA (hydroxyapatite), but calcium oxalate (undifferentiated) might be also detected in some samples. However, Raman spectral results could detect three components, HA, COM (calcium oxalate monohydrate) or COD (calcium oxalate dihydrate) separated in nine samples. Different compositions in the prostatic calculi were obtained by both spectroscopic detections with manual single-point random analysis implying that both manually traditional methods were failed to provide the real chemical composition of the prostatic calculi in a short time. The FTIR microscopic mapping system via point-by-point mapping analysis evidenced that it could rapidly detect all the complicated components distributed within the prostatic calculi rather than uncertain components detected by traditional FTIR or Raman microspectroscopy. More studies should be carried out in future. This preliminary result suggests that the FTIR mapping better characterizes the stone composition over single-point FTIR and Raman microscopic analysis in prostatic calculi.

Keywords Prostatic calculi · FTIR · Raman · Microscopic mapping · Hydroxyapatite · Calcium oxalate monohydrate · Calcium oxalate dihydrate

T. H.-S. Hsu
Division of Urology, Department of Surgery, Lotung Pohai Hospital, Lotung, Yilan, Taiwan, ROC

S.-Y. Lin (✉) · C.-C. Lin · W.-T. Cheng
Department of Biotechnology, Yuanpei University, Hsin-Chu, Taiwan, ROC
e-mail: sylin@mail.ypu.edu.tw

Introduction

Prostatic calcification is constructed by the deposition of calcareous material within the tissues or acini of the prostate gland, and it has been proposed to be associated with the formation of prostatic hyperplasia and carcinoma [1–3]. Because prostatic lithiasis has been reported to closely relate to the occurrence of inflammation [3, 4], knowing the chemical composition of prostatic calculi is of great importance for pathogenesis of prostatic lithiasis using an optimal analytical method. Parallels to the analysis of kidney stones [5–8], numerous analytical methods have also been applied to determine the chemical compositions of prostatic calculi [8–11].

Fourier transform infrared (FTIR) spectroscopy is one of the most traditional techniques for the calculi analysis [8–10]. FTIR spectral analysis allows identifying any organic or inorganic molecules in the calcified samples. In the traditional FTIR analysis, the calculi sample was either ground with KBr powder or sealed within two KBr pellets

and then pressed to form a KBr disc for spectral determination [5, 6, 8–15]. However, the traditional FTIR analysis fails to reflect the spatial distribution of the complicated components in the calcified mixture using a manually single-point random determination. The heterogeneous distribution of the components within KBr disc may cause an incorrect conclusion by few sampling points through this traditional spectral analysis.

A powerful FTIR microspectroscopic mapping system is becoming an increasingly unique technique in biomedical application [16, 17]. This technique combining the light microscopy, FTIR spectroscopy and a mapping stage provides spatially resolved information on the basis of the chemical composition of the different structural components. This mapping stage can freely move the sample along the *X* and *Y* axes into the microscope's beam path. The IR spectra of different components located in the sample's microstructure can possibly be determined via point-by-point mapping analysis. The aim of this preliminary study was attempted to evaluate the feasibility of FTIR microspectroscopic mapping system to rapidly screen and detect the real composited components contained in the prostatic calculi. As a comparison, the calculi samples were also determined by the traditional FTIR and Raman microspectroscopies by a manual single-point random analysis.

Materials and methods

Patients

Prostatic calculi were retrieved by prostatic chips during transurethral resection of the prostate (TURP) from nine patients diagnosed having benign prostatic hyperplasia with lower urinary tract symptoms. The mean age of 9 patients was 76 (range 61–91) years. The level of serum prostatic-specific antigen was within 0–12.63 ng/ml. Patients with known prostatic cancer were excluded. The calculi samples were isolated, washed with double distilled water for two times, and then sent for the histopathological examination and spectral analysis. This study was approved by the Institutional Review Board at the Lotung Pohai Hospital according to the declaration of Helsinki.

Materials

Hydroxyapatite (HA, $Ca_{10}(PO_4)_6(OH)_2$), calcium oxalate monohydrate (COM, $CaC_2O_4\ H_2O$) and calcium oxalate dihydrate (COD, $CaC_2O_4\ 2H_2O$) as standard references were purchased from Nacalai Tesque, Inc. (Tokyo, Japan), and used without further purification.

Sample preparation for FTIR analysis

Different prostatic calculi samples stored at 25°C, 50% RH conditions were previously crushed and ground by an agate mortar and pestle for 1 min to achieve a fine particle. A trace amount of fine ground calculi powders was sealed within two KBr pellets by a hydraulic press under 400 kg/cm^2 compression pressure for 15 s to form a KBr disc [14, 15]. The fine powder distributed within KBr disc was observed and photographed by infrared microscope (IRT-5000-16, Jasco Co., Tokyo, Japan) with a video camera.

Vibrational microspectroscopic single-point determination

Each KBr disc prepared from different patients was examined to determine the chemical component using an FTIR microspectroscopy (IRT-5000-16/FTIR-6200, Jasco Co.) equipped with an MCT detector via a transmission technique [21–23]. The IR spectra over the range of 2,000–650 cm^{-1} were carried out at 200 scans under a resolution of 4 cm^{-1} and the analytical spot size of sample was set at 100 × 100 μm through aperture of microscope. The same sample size for FTIR determination was also directly and randomly determined by a confocal micro-Raman spectrophotometer (Ventuno, Jasco Co.) equipped with a laser power of 30 mW green (532 nm) solid-state laser [14, 18]. The operational conditions of Raman system over the range of 2,000–200 cm^{-1} were controlled with 10-s integration time and 60 scans by providing 4 cm^{-1} spectral resolution. On the CCD detector array, the wavenumbers were spaced 1.3 cm^{-1} per pixel. Both traditional FTIR and Raman spectral analyses were randomly detected via a manual single-point determination.

Microspectroscopic FTIR mapping study

One KBr disc prepared from the representative sample b was also set on the stage of FTIR microscopic spectrometer (IRT-5000-16/FTIR-6200, Jasco Co.). The system was operated in a transmission mode over the range of 2,000–650 cm^{-1}. An appropriate sample area was selected, and the IR spectra were collected successively from the actual analysis area by an automatic XYZ mapping stage (IPS-5000, Jasco Co.). This mapping stage was employed to obtain full IR spectra of calculi sample at any random area of KBr disc through whole area by point-by-point mapping [19]. The sampling aperture was set at 100 × 100 μm, each spectrum was performed at 100 scans with the resolution of 4 cm^{-1}. The map of size was 10 × 10 points in 1 mm^2, leading to the acquisition of 100 spectra.

Results

The traditional FTIR and Raman spectra of standard references of HA, COM and COD by a manual single-point determination are shown in Fig. 1. The FTIR and Raman vibrational frequencies and assignments of theses standard references were also listed in Table 1 [6, 13, 20–23]. The IR spectrum of HA indicates typical IR absorption peaks at 1,092, 1,031 and 961 cm^{-1} corresponding to the v_3 and v_1 stretching modes of phosphate and a weak absorbance at 873 cm^{-1} arising from the hydrogen phosphate [5–7, 22–26]. A strong peak at 963 cm^{-1} in the Raman spectrum was mainly due to the v_1 stretching mode of phosphate of HA, but 4 weak peaks at 1,076, 1,042, 588 and 427 cm^{-1} were separately assigned to v_3, v_4 and v_2 vibrations in the phosphate groups [24, 27]. Three strong peaks at 1,619, 1,320 and 780 cm^{-1} were observed in the IR spectrum of COM, but two strong IR peaks at 1,627 and 1,327 cm^{-1} with one weak peak at 781 cm^{-1} were characterized in the IR spectrum of COD (Fig. 1b, c). The strong bands at 1,619 (1,627) and 1,320 (1,327) cm^{-1} were, respectively, assigned to the asymmetric and symmetric COO^- stretching of coordinated oxalate groups [20, 28]. The peak at 780 (781) cm^{-1} was due to the out-of-plane C–O deformation [26, 29], while the intense Raman spectral doublet for COM was located at 1,497/1,468 cm^{-1} due to the symmetric COO^- stretching vibration. Other less intense Raman peaks at 1,630, 895 and 502 cm^{-1} were assigned to the asymmetric COO^- stretching, C–C stretching and O–C–O in plane bending for COM, respectively [30]. The peak at 596 or 598 cm^{-1} was broad with low intensity, and also attributed to water libration mode [21]. On the other hand, a sharp singlet near 1,476 cm^{-1} corresponded to symmetric COO^- stretching and a less intense peak at 912 cm^{-1} due to the shifted C–C stretching mode were found in the Raman spectrum of COD [6, 28, 30].

Figure 2 shows the traditional FTIR and Raman spectra of the prostatic calculi isolated from nine patients by a manual single-point random analysis. From the appearance of 1,417, 1,320 and 781 cm^{-1}, it clearly indicates that all the IR spectra seemed to be approximately classified into three groups, group I (*a–c*), group II (*d–f*) and group III (*g–i*). Several unique IR peaks at 1,417 cm^{-1} corresponded to the asymmetric stretching of carbonate of HA, at 1,095 (1,098), 1,031, 962 (961) cm^{-1} attributed to the stretching of phosphate of HA, at 1,320 cm^{-1} assigned to the symmetric COO^- stretching band of the oxalate anion, and at 781 cm^{-1} due to out-of-plain C–O deformation of oxalates suggest that nine calculi samples mainly consisted of carbonated HA, but calcium oxalate (undifferentiated) was only detected in some samples via a single-point FTIR determination [6, 20, 26, 28].

In addition, the Raman spectra obtained by single-point determination seemed to be separated into three groups from the appearance of Raman peaks at 961–965 cm^{-1} (*a–f*), 1,477 cm^{-1} (*f*) and a doublet at 1,493/1,468 cm^{-1} (*g–i*). Samples *a–c* revealed typical Raman spectral pattern of HA at 1075 (v_2 carbonate of HA), 961–965 and 585–592 cm^{-1}, suggesting the composition of samples *a–c* was mainly constructed by carbonated HA. Samples *d–e* consisted of HA due to only the appearance of the peak at 963 cm^{-1}. However, sample *f* was found to have two Raman patterns, one was mainly contained by HA (963 cm^{-1}) but another was constructed by COD (1,477, 912, 870, 600 and 508 cm^{-1}). While COM (1,493/1,468, 909 and 508 cm^{-1}) and HA (965 cm^{-1}) were presented in the Raman spectra of samples *g–i*. This indicates again that different complicated components were detected from the prostatic calculi by a manual single-point random analysis.

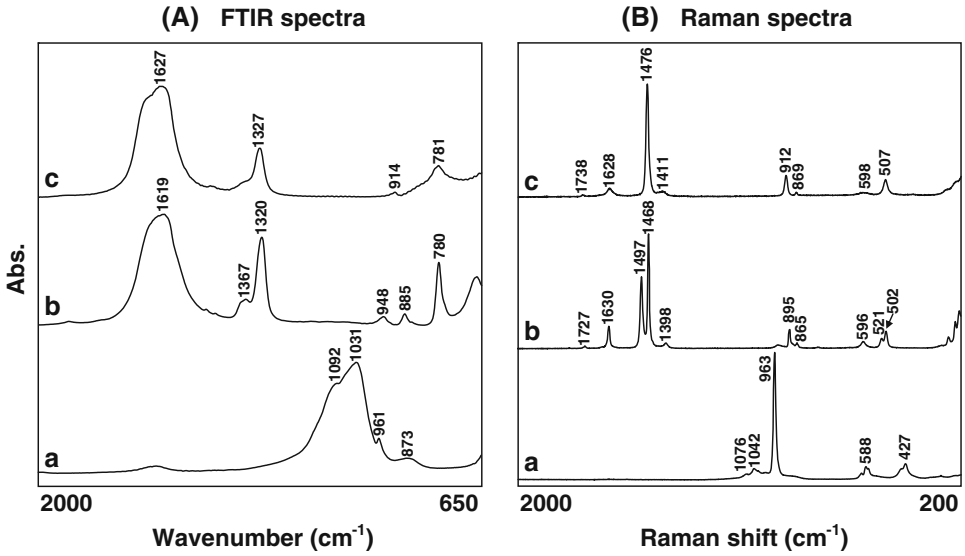

Fig. 1 FTIR and Raman spectra of pure reference substances of HA (**a**), COM (**b**) and COD (**c**) by a manual single-point random determination

Table 1 FTIR and Raman vibrational frequencies and assignments of the standard references of HA, COM and COD [6, 13, 20–23]

HA		COM		COD		Assignments
IR	Raman	IR	Raman	IR	Raman	
		1619	1630	1627	1628	Asymmetric COO^- stretching
			1497			Symmetric COO^- stretching
					1476	Symmetric COO^- stretching
			1468			Symmetric COO^- stretching
		1320		1327		Symmetric COO^- stretching
1092	1076					v_3 stretching of phosphate
	1042					v_3 stretching of phosphate
1031						v_3 stretching of phosphate
961	963					v_1 stretching of phosphate
		948		914	912	Shift C–C stretching
		885	895			C–C stretching
873						Hydrogen phosphate
		780		781		Out-of-plane C–O deformation
			596		598	Water libration
	588					v_4 stretching of phosphate
			502		507	O–C–O in plain bending
	427					v_2 stretching of phosphate

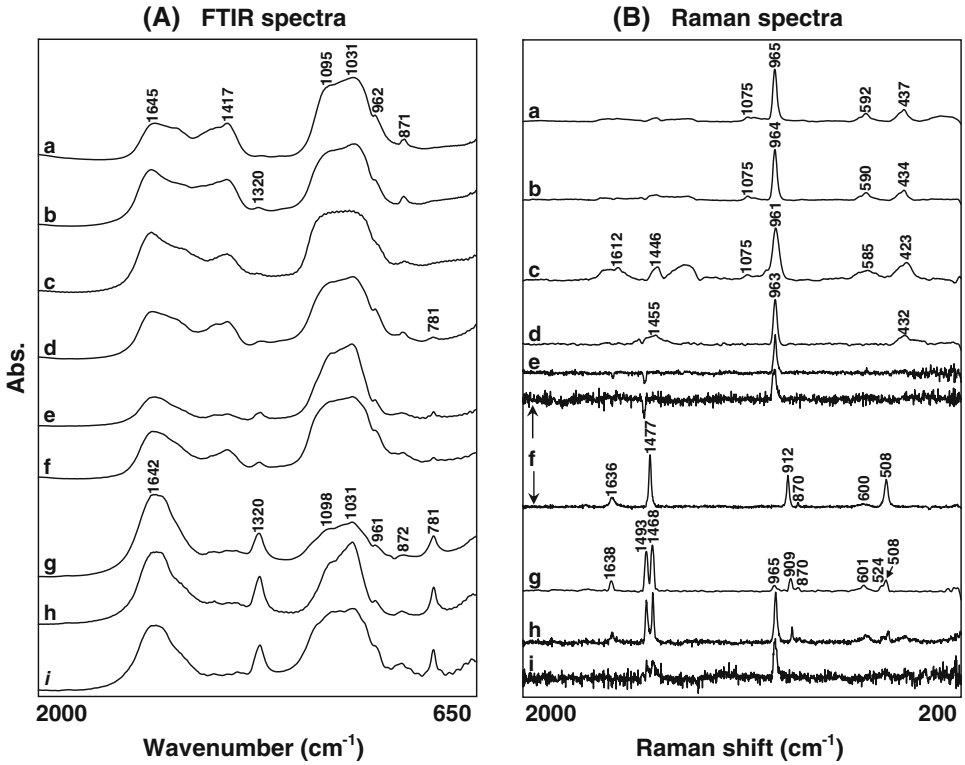

Fig. 2 FTIR and Raman spectra of the prostatic calculi isolated from nine patients (*a–i*) by a manual single-point random determination

Figure 3 shows the representative IR line spectra collected from mapping stage of fine ground powders (sample *b,* as an example) sealed within two KBr pellet (A), optical image (B), and spectroscopic image plane representing the area under the IR peaks at 781 cm^{-1} of a sample (C). The area of red line was the area for mapping. It clearly illustrates that some IR spectra were found to have a spectral peak at 781 cm^{-1}, which was assigned to calcium oxalate. Several IR spectra had also exhibited a peak at 1,320 cm^{-1} due to calcium oxalate. However, many IR spectra did not

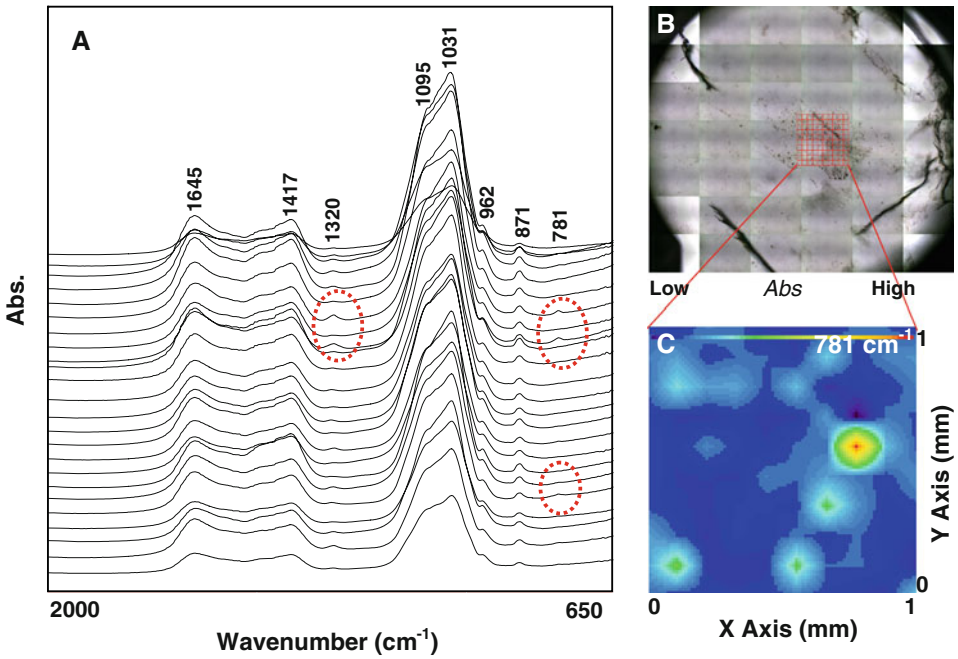

Fig. 3 The representative IR line spectra collected from mapping stage of fine ground powders (sample *b,* as an example) sealed within two KBr pellet (**A**), optical image (**B**), and spectroscopic image plane representing the area under the IR peaks at 781 cm^{-1} of a sample (**C**). *Key* the area shown is 1.0 × 1.0 mm. *Red areas* represent the highest absorbance, while *blue areas* denote low IR absorbance+

show above two peak positions. From these IR spectra determined by point-by-point mapping analysis, sample *b* was constructed by carbonated HA (1,417 cm^{-1}), HA (1,095 and 1,031 cm^{-1}) and calcium oxalate (1,320 and 781 cm^{-1}), which was significantly different from that of FTIR and Raman spectra of sample *b* by a manual single-point determination (Fig. 2b).

Discussion

FTIR and Raman spectroscopies are complementary techniques to examine the fundamental molecular vibrations of samples, although their selection rules for the molecules are different: one is the changes in dipole moment and another is the changes in polarizability [31]. Since some vibrations of molecules may be strong in IR spectra, but weak in Raman spectra and vice versa, thus it may possibly reveal different chemical compositions of prostatic calculi for nine patients as shown in Fig. 2. From the manual single-point random determination of FTIR spectra, the samples *a–c* only consisted of carbonated HA, but the samples *d–i* were made of carbonated HA and calcium oxalate, in which the calcium oxalate could not be differentiated from COD or COM. From Raman spectra determined by a manual single-point random analysis, however, the samples *a-c* were only constructed by carbonated HA and samples *d–e* consisted of HA alone. The sample *f* was contained by HA and/or COD, whereas the samples *g–i* were composed of HA and COM. Obviously, both spectroscopic determinations resulted in different compositions from the prostatic calculi, indicating each manual single-point random analytical method was not sufficient to provide the available information of the calculi composition at any time. Both vibrational spectroscopies should be applied together by many times; otherwise the conclusion may be possibly incorrect.

To synchronously identify the real chemical compositions of prostatic calculi, the FTIR microspectroscopic mapping system was easily applied to show the distribution of chemical components in the calcified tissue by one-step determination. The characteristic absorption bands were obtained to localize and identify component itself. The FTIR mapping system exhibited the real components in the prostatic calculi rather than uncertain components determined by traditional FTIR or Raman microspectroscopy. Figure 3C also indicates the IR absorbance image representing the area under the IR peak at 781 cm^{-1} for a sample *b*. The red areas represent the highest absorbance with higher content, whereas the deep blue areas denote low IR absorbance. Because the peak at 781 cm^{-1} represented the existence of calcium oxalate, the non-uniform color display revealed the heterogeneous distribution of calcium oxalate in the calculus. If the traditional FTIR or Raman microspectroscopy was used alone, the manual single-point random analysis was difficult to homogeneously measure each sample point within KBr disc leading to an inaccurate conclusion. The feasibility of mapping system applied to the defined area of sample could completely examine the detailed components of the sample by the point-by-point mapping analysis from area determination.

Conclusions

The preliminary results demonstrate the feasibility of using the FTIR spectroscopic mapping system to rapidly screen and accurately detect the composited components in prostatic calculi, the application of both FTIR and Raman microscopic mapping systems will be studied in future.

Conflict of interest None.

References

1. Klimas R, Bennett B, Gardner WA Jr (1985) Prostatic calculi: a review. Prostate 7:91–96
2. Shoskes DA, Lee CT, Murphy D, Kefer J, Wood HM (2007) Incidence and significance of prostatic stones in men with chronic prostatitis/chronic pelvic pain syndrome. Urology 70:235–238
3. Cristol DS, Emmett JL (1944) Incident of coincidence prostatic calculi, prostatic hyperplasia and carcinoma of prostate gland. JAMA 124:646–647
4. Sfanos KS, Wilson BA, De Marzo AM, Isaacs WB (2009) Acute inflammatory proteins constitute the organic matrix of prostatic corpora amylacea and calculi in men with prostate cancer. Proc Natl Acad Sci USA 106:3443–3448
5. Daudon M, Bader CA, Jungers P (1993) Urinary calculi: review of classification methods and correlations with etiology. Scanning Microsc 7:1081–1106
6. Carmona P, Bellanato J, Escolar E (1998) Infrared and Raman spectroscopy of urinary calculi: a review. Biospectroscopy 3:331–346
7. Bouropoulos N, Bouropoulos C, Klepetsanis PG, Melekos M, Barbalias G, Koutsoukos PG (1996) A model system for the investigation of urinary stone formation. Br J Urol 78:169–175
8. Evan AP, Coe FL, Lingeman JE, Shao Y, Sommer AJ, Bledsoe SB, Anderson JC, Worcester EM (2007) Mechanism of formation of human calcium oxalate renal stones on Randall's plaque. Anat Rec 290:1315–1323
9. Krafft C, Steiner G, Beleites C, Salzer R (2009) Disease recognition by infrared and Raman spectroscopy. J Biophotonics 2:13–28
10. Stothers L, Shadgan B, Macnab A (2008) Urological applications of near infrared spectroscopy. Can J Urol 15:4399–4409
11. Kodaka T, Hirayama A, Sano T, Debari K, Mayahara M, Nakamura M (2008) Fine structure and mineral components of primary calculi in some human prostates. J Electron Microsc (Tokyo) 57:133–141
12. Jesús Fernández-Almeida, Ana Fernández-Gacio, Marcos Carlos F, Maira Fernández-Gacio (2003) Infrared spectroscopy in the study of renal lithiasis. J Chem Educ 80:909–910
13. Khalil SKH, Azooz MA (2007) Application of vibrational spectroscopy in identification of the composition of the urinary stones. J Appl Sci Res 3:387–391
14. Chen KH, Cheng WT, Li MJ, Yang DM, Lin SY (2005) Calcification of senile cataractous lens determined by Fourier transform infrared (FTIR) and Raman microspectroscopies. J Microsc 219:36–41
15. Chiou HJ, Hung SC, Lin SY, Wei YS, Li MJ (2010) Correlations among mineral components, progressive calcification process and clinical symptoms of calcific tendonitis. Rheumatology 49:548–555
16. Guilment J, Markel S, Windig W (1994) Infrared chemical microimaging assisted by interactive self-modeling multivariate analysis. Appl Spectrosc 48:320–326
17. Wetzel DL, LeVine SM (1999) Imaging molecular chemistry with infrared microscopy. Science 285:1224–1225
18. Hsu TH, Lin SY, Lin CC, Cheng WT, Li MJ (2009) Spectral diagnosis and analysis of a superior vesical artery calcification. Urol Res 37:253–256
19. Lee TH, Lin SY (2004) Microspectroscopic FT-IR mapping system as a tool to assess blend homogeneity of drug-excipient mixtures. Eur J Pharm Sci 23:117–122
20. Estepa L, Daudon M (1997) Contribution of Fourier transform infrared spectroscopy to the identification of urinary stones and kidney crystal deposits. Biospectroscopy 3:347–369
21. Frost RL (2004) Raman spectroscopy of natural oxalates. Anal Chim Acta 517:207–214
22. Koutsopoulos S (2002) Synthesis and characterization of hydroxyapatite crystals: a review study on the analytical methods. J Biomed Mater Res 62:600–612
23. Sadat-Shojai M (2009) Preparation of hydroxyapatite nanoparticles: comparison between hydrothermal and solvo-treatment processes and colloidal stability of produced nanoparticles in a dilute experimental dental adhesive. J Iran Chem Soc 6:386–392
24. Nakamoto K (1997) Infrared and Raman spectra of inorganic and coordination compounds, part A and B. applications in coordination, organometallic, and bioinorganic chemistry, 5th edn. Wiley, New York
25. Boskey AL, Mendelsohn R (2005) Infrared spectroscopic characterization of mineralized tissues. Vib Spectrosc 38:107–114
26. Herman RG, Bogdan CE, Sommer AJ, Simpson DR (1987) Discrimination among carbonate minerals by Raman spectroscopy using the laser microprobe. Appl Spectrosc 41:437–440
27. Aminzadeh A, Shahabi S, Walsh LJ (1999) Raman spectroscopic studies of CO_2 laser-irradiated human dental enamel. Spectrochim Acta A Mol Biomol Spectrosc 55A:1303–1308
28. Kontoyannis CG, Bouropoulos NC, Koutsoukos PG (1997) Urinary Stone Layer Analysis of mineral components by Raman spectroscopy, IR spectroscopy, and X-ray powder diffraction: a comparative study. Appl Spectrosc 51:1205–1209
29. Kanchana G, Sundaramoorthi P, Jeyanthi GP (2009) Bio-chemical analysis and FTIR-spectral studies of artificially removed renal stone mineral constituents. J Miner Mater Character Eng 8:161–170
30. Kontoyannis CG, Bouropoulos NC, Koutsoukos PG (1997) Use of Raman spectroscopy for the quantitative analysis of calcium oxalate hydrates: application for the analysis of urinary stones. Appl Spectrosc 51:64–67
31. Ellis DI, Goodacre R (2006) Metabolic fingerprinting in disease diagnosis: biomedical applications of infrared and Raman spectroscopy. Analyst 131:875–885